Heliyon 7 (2021) e08020

Contents lists available at ScienceDirect

Heliyon

journal homepage: www.cell.com/heliyon

Research article

Theory of coupled resistive drift and resistive drift ballooning instabilities in fusion plasma

Umer Rehman [a,*], Ahmad Ali [b], Shakeel Mahmood [a]

[a] Department of Physics, Air University, E-09 Complex, Islamabad, 44000, Pakistan
[b] National Tokamak Fusion Program, Islamabad, 44000, Pakistan

ARTICLE INFO

Keywords:
Drift wave
Fusion plasma
Plasma instability
Coupled modes

ABSTRACT

Drift wave instabilities (DWI) associated with the two-fluid dynamics seems to be responsible for anomalous transport in modern day tokamaks. Ballooning instabilities tend to exchange flux tubes of different pressure, resulting in convective transport. The micro-level turbulence (drift wave) is coupled with the macro-level (ballooning mode) dynamics in fusion experiments. The co-existence of DWI and drift ballooning instabilities (DBI) is discussed in this work using a four-field plasma model. The formulation preserves both the microscopic and macroscopic dynamics of plasma. To demonstrate the coupling, a new dispersion relation is derived to analyze stability of the coupled modes in a non-uniform magnetized plasma. Linear stability of coupled drift-ballooning and drift-acoustic modes have been explored. The two-fluid effect (micro-level influence) through diamagnetic drift frequency for electrons and curvature drift frequency on unstable modes are demonstrated.

1. Introduction

Drift wave turbulence is considered a natural cause of anomalous transport (due to pressure gradient), specifically in the tokamak edge plasma region (Liewer 1985; Callen 1977; Hasegawa and Wakatani 1982; Wakatani and Hasegawa 1984; Graessle et al., 1989; Horton 1990; Park et al., 2018). Whereas, curvature of the magnetic field triggers a centrifugal force due to thermal motion along the field lines. In the scenario, when the direction of curvature vector aligned against the direction of pressure gradient, the ballooning mode becomes unstable. The effective gravitational force may be used to simulate a magnetic field curvature (Weiland 2000).

In previous studies (Hasegawa and Mima 1977, 1978; Waltlz 1985; Biskamp and Walter 1985; Scott 1990; Scott et al. 1991), the drift wave turbulence in slab geometry for sheared magnetic fields and all its fundamental phenomena were investigated. Initially, two fluid equations (Galeev et al., 1964) with electrostatic approximation were used to explore the DWI. Later, Scott (1997) introduced the magnetic field perturbation through the parallel component of the vector potential. A series of articles (Lee et al., 2015; Lee et al. 2015; Lee et al. 2015) have been written on DWI under the blob's dynamics in fusion plasmas. The authors demonstrated the electromagnetic (EM) effects of the resistive drift mode (RDM) on the filaments/blobs and turbulence in the fusion plasma. To comprehend the dynamics of fusion plasma, significant study has been done on blobs (L. Easy et al., 2014; Bisai et al., 2019; Furno et al., 2008). In drift waves, free energy is extracted from the background-gradient, which contributes to the parallel current and establishes an adiabatic coupling. On the other hand in the ballooning mode, a well-known Alfvenic coupling is associated with $B \cdot \nabla\varphi$ potentials and it permits the free energy to infiltrate $\boldsymbol{E} \times \boldsymbol{B}$eddies.

Using MHD models, the resistive ballooning turbulence and the ideal ballooning modes were investigated by several researchers (Strauss 1976; Fridberg 2014; Kikuchi and Azumi 2015; Todd et al., 1976; Strauss 1976; Dewar and Glasser 1983; Hirose et al. 1994; Connor et al. 1998; Hegna and Hudson 2002; Coppi 1977). The adiabatic coupling response is ignored in the ballooning mode due to smallness of $k_{\|}$ or by considering a strictly impeded parallel propagation so that the resistive Alfvenic wave dampens towards the zero completely. The only possibility is that the free-energy can be transferred to E-cross-B from back-ground gradient through magnetic field line curvature in the MHD formalism, and it gives rise to the well-known ballooning. In the toroidal orientation, it is known as ballooning mode and it is destabilized in the outer part of the nested tori surfaces, where the radius of curvature (usually known as bad curvature) vectors align opposite to the pressure gradient. The dynamical form of this instability was discussed in order to explain non-typical observation of magnetic perturbations located on the outer side of the

* Corresponding author.
E-mail address: umer@mail.ustc.edu.cn (U. Rehman).

https://doi.org/10.1016/j.heliyon.2021.e08020
Received 1 June 2021; Received in revised form 30 August 2021; Accepted 15 September 2021

Princeton Large Tokamak (Dobrott et al. 1977). These perturbations were narrated as the ideal ballooning mode and were treated traditionally (Connor et al., 1978; Strauss 1981; Carreras et al. 1983) together with ballooning transformation (Hender et al. 1984; Sykes et al. 1987). However, the resistive ballooning mode (RBM) was introduced to explain the existence of tokamak edge transport within the ideal limit of plasma β and at the amplitudes of mode that are implausible by the existing free energy channels (Carreras et al. 1987, 1989; Camargo et al. 1995; Hastie et al. 2003; Rafiq et al. 2009; McCarthy et al. 1992). The study of ballooning modes were expanded by including the two-fluid generalized Ohm law gave rise to the microscopic ballooning mode to the edge transport mode (Guzdar et al. 2001; Zeiler et al. 1996; Rogers and Drake 1997; Xu et al. 2000), which coincided with previous methods constructed for ballooning modes (Cowley et al. 1991; Beer et al. 1995).

The coexistence of the microscopic level drift wave and the macroscopic level ballooning mode in the fusion plasmas can give rise to hybrid unstable modes. The $\boldsymbol{E}\times\boldsymbol{B}$ turbulence in the presence of background pressure-gradient can destabilize both types of modes. These two modes are distinct because of the different energy transfer channels, i.e. parallel dynamics in case of DWI and curvature forcing in case of RBM. The MHD model restrains the ballooning mechanism but neglects the drift wave propagation by missing adiabatic coupling. Such adiabatic coupling can be incorporated in four field plasma model. The slab drift wave formalism omits the ballooning mechanism by neglecting the magnetic curvature effects. The effective gravitational force is used to simulate a magnetic curvature in our model. In the presence of a non-uniform magnetic field, linear drift waves predominantly lead to finite current divergence (FCD) in the parallel dynamics. This FCD is causing departure from the adiabatic state, and phase shift occurs across a broader range of plasma parameters. This phenomenon is giving rise to drift resistive ballooning modes, which was originally obtained at the order of diamagnetic frequencies (Camargo et al. 1995).

In the tokamak plasma edge region, the localized pressure gradient is not sufficient to drive the ideal MHD modes. Therefore, the localized instability in the plasma edge seems to be inconsistent with prediction of linear ideal ballooning mode (Hubbard et al. 2001). The edge conditions are thought to be cold enough for the collision frequency to be faster than the turbulence and pressure remains low enough for the magnetic activity associated with the plasma current fluctuations. These edge regimes were confirmed in experiments (Wootton et al. 1990; Bessenrodt-Weberpals et al. the ASDEX Team 1993). Although, there are many studies devoted to explain instability in edge region (Myra et al. 2000; Rogers and Drake 1999; Xu et al. 2000; Xu and Cohen, 2000; Rehman 2019; Mikhailovskii and Rudakov 1963), however, in explaining these localized instabilities, the role of the coupled macro and micro-mode were ignored. Recently, Xu et al. (2021) has demonstrated Impurity effect on drift-resistive-inertial ballooning mode and associated transport at the edge of tokamak plasmas.

In current investigation, a set of Braginskii equations are being presented, which include all macroscopic and microscopic plasma dynamics to estimate the growth of the coupled unstable modes. The key effects associated with the tokamak edge plasma environment such as two-fluid effects (ion curvature drift, electron diamagnetic drift), dissipation effect (the resistivity due to collision) and the coupling effect due to interaction with acoustic mode are incorporated in the four-field plasma model. To find the growth, a dispersion relation is derived with the ordering$\Omega \sim \Omega_s \sim \Omega_{*i} \sim \Omega_{*e} \sim \Omega_\kappa \sim \eta k_\perp^2$. Here, Ω is frequency of the mode, $\Omega_s = C_s/L$ is sound wave propagation frequency (where, $C_s = \sqrt{(T_i + T_e)/m_i}$ and L is characteristic length), $\Omega_{*j} = \{(\nabla p_j)/neB^2\}\cdot(k\times B)$ is the diamagnetic frequency for j species, $\Omega_\kappa = \{(\nabla p_j \times B)/neB^2\}\cdot\kappa$ is the ion drift frequency due to magnetic curvature/gradient (where $\kappa = \{(B/B)\cdot\nabla\}(B/B)$), and η is the Spitzer resistivity.

The rest of manuscript is organized in following manner. Section 2 is allocated for the description of equilibrium magnetic field and governing equations. In Section 3, analytic treatment has been carried out to obtain a generalized dispersion relation. Section 4 contains results of coupled modes, and finally a brief summary of the work is presented.

2. Theory

To describe geometry, we have considered the magnetic field curvature in the xz-plane and the magnetic field is allowed to vary slightly along the x-axis. This configuration mimics the radial inhomogeneities in plasma and magnetic field in toroidal magnetic field devices such as tokamak, stellarator and reverse field pinches. It is assumed that an equilibrium magnetic field$\mathbf{B}_0 = B_0(x)[\hat{z} + (x/L_B)\hat{y}]$, with a dominant field along z-direction and sheared field about rational surface$(x = a - a_s, q(a_s) = m/n$, where m and n are integers). Here, $L_B^{-1} = \kappa = 1/B_0 dB_y/dx$ is the inverse magnetic sheared length. With this local equilibrium magnetic field, the magnetic curvature (i.e. $dB_0/dx \neq 0$) is allowed. A simple reduced set of two-fluid equations are given in (Hastie et al. 2003; Rafiq et al. 2009; Zeiler et al. 1997). Using the equations 31-36 (given in Zeiler et al. 1997) with assumption that isothermal electron and ions are embedded in the magnetic field, the following set of equations is obtained for the four adimensional perturbed fields as a four field plasma model of coupled modes. The momentum equation, equation of vorticity, electron continuity equation and generalized Ohm's law are given as;

$$\rho\frac{d\boldsymbol{U}}{dt} = -\nabla(p_i + p_e) + \boldsymbol{j}\times\boldsymbol{B} - \rho\mathbf{g}_{\text{eff.}} - \nabla\cdot\pi_i \tag{1}$$

$$\nabla\cdot N\left(\boldsymbol{U_{pi}} + \boldsymbol{U_{\pi i}} + \boldsymbol{U_\kappa}\right) + \nabla\cdot N(\boldsymbol{U_{*i}} - \boldsymbol{U_{*e}}) + \nabla\cdot\left(N\boldsymbol{U_{pe}}\right) + \frac{1}{e}\nabla_\parallel j_\parallel = 0 \tag{2}$$

$$\frac{\partial N}{\partial t} + \nabla\cdot N(\boldsymbol{U_E} - \boldsymbol{U_{*e}}) + \nabla\cdot N\left(\boldsymbol{U_{pe}} - \boldsymbol{U_\eta}\right) + \nabla\cdot(NU_{\parallel e}) = 0 \tag{3}$$

$$\boldsymbol{E} = -\boldsymbol{U}\times\boldsymbol{B} + \frac{1}{Ne}(\boldsymbol{j}\times\boldsymbol{B}) - \nabla p_e + \eta\boldsymbol{j} + \frac{m_e}{e^2N}\frac{\partial\boldsymbol{j}}{\partial t} \tag{4}$$

Where$\boldsymbol{\rho}$ is the mass density, $\boldsymbol{U}$ is velocity of the fluid flow (consists of electron and ion), first term on right hand side (r.h.s) is scalar pressure consists of electron and ion while the off-diagonal terms are neglected for electron due to short relevant length scale. Further, ion viscous force is incorporated as last term on r.h.s in momentum balance Eq. (1), in above equations j is the current density, while all other symbols are usual meaning, and the third term on r.h.s is the force due to effective gravity, which is used as the simulator of the curvature. In the set of equations,$\boldsymbol{U_E} = (-c/B)\nabla\varphi\times\tilde{\boldsymbol{B}}$ is the E × B drift,$\boldsymbol{U_{*j}} = (-c/Nq_jB)\nabla p_j\times\tilde{\boldsymbol{B}}$ is the diamagnetic drift for jth species, $\boldsymbol{U_{\pi i}} = (-c/NeB)\nabla\cdot\pi_i\times\tilde{\boldsymbol{B}}$ is the ion viscous drift (where π_i is the ion stress tensor), $\boldsymbol{U_\eta} = (\boldsymbol{c}/\boldsymbol{NeB})\boldsymbol{R}\times\tilde{\boldsymbol{B}}$is resistive drift contribution (where $\mathbf{R} = \boldsymbol{\eta e^2 N}(\mathbf{U_i} - \mathbf{U_e})$ represents the frictional force contain fluid velocity of electron$\boldsymbol{U_e} = \boldsymbol{U_E} + \boldsymbol{U_{*e}}$, which is colliding the ions, hence, spitzer resistivity $\boldsymbol{\eta}$ is incorporated in the model through resistive force), $\boldsymbol{U_\kappa} = \left\{\left(-\frac{c}{NeB}\right)\nabla p_i\cdot\kappa\right\}\times\tilde{\boldsymbol{B}}$ is curvature drift, where $\boldsymbol{\kappa}$retain the drift due to effective gravitation force taken into account in the model. Here, the expression for the effective gravitational force is $\boldsymbol{\rho g_{\text{eff.}}} = \{2N(\mathbf{T_i} + \mathbf{T_e})/\mathbf{B}\}\mathbf{dB\hat{x}}/\mathbf{dx}$. The quantity g is chosen in such a way that the gravitational drift of the ions same as the centrifugal drift, and $\boldsymbol{U_{pj}} = (1/\omega_{cj})\{\partial/\partial t + U_j\}U_j\times\tilde{\boldsymbol{B}}$ is the polarization drift of jth species. Isothermal electrons and ions$\boldsymbol{T} = \boldsymbol{T_e} = \boldsymbol{T_i}$ are considered. Here,$\tilde{\boldsymbol{B}} = \mathbf{B}/|\mathrm{B}|, j_\parallel$ is the plasma current parallel to the magnetic field and Using parallel component of generalized Ohm's law (4) and assuming constant temperature along field:

$$E_\parallel = \eta j_\parallel - T_e\nabla_\parallel N + \frac{m_e}{e^2N}\frac{\partial j_\parallel}{\partial t} \tag{5}$$

Using $E_{\parallel} = -\nabla_{\parallel}\varphi - (1/c)\partial A_{\parallel}/\partial t$, and assuming quasi-neutrality condition $N = N_e = N_i$, Ampere's law is expressed as,

$$\nabla_{\perp}^2 A_{\parallel} = \frac{-4\pi}{c} j_{\parallel}, \tag{6}$$

Using above expression, Eqs. (1), (2), (3), and (4) are linearized with respect to perturbations proportional to $\mathbf{exp}[-\imath(\Omega t + \boldsymbol{k}\cdot\boldsymbol{r})]$, which result in four equations (for the four perturbed fields' quantities) as follows;

$$(\Omega - \Omega_{\kappa})\tilde{U}_{\parallel} + \Omega_{*e}\tilde{\chi} - C_s k_{\parallel}\tilde{N} + 4i\mu k_{\perp}^2 \tilde{U}_{\parallel} = 0, \tag{7}$$

$$\Omega k_{\perp}^2 \rho_i^2(\tilde{\varphi} + \tilde{N}) - 4\Omega_{\kappa}\tilde{N} - \frac{C_A^2}{C_s} k_{\parallel}\left(k_{\perp}^2\rho_i^2\tilde{\chi}\right) + i\mu k_{\perp}^4 \rho_i^2(\tilde{\varphi} + \tilde{N}) = 0, \tag{8}$$

$$\left(\Omega + \Omega k_{\perp}^2\rho_i^2\right)\tilde{N} + \left(\Omega k_{\perp}^2\rho_i^2 - \Omega_{*e}\right)\tilde{\varphi} - C_s k_{\parallel}\tilde{U}_{\parallel} + i\eta\frac{C_A^2}{C_s^2}\tilde{N} = 0, \tag{9}$$

$$(\Omega - \Omega_{*e})\tilde{\chi} - C_s k_{\parallel}(\tilde{\varphi} + \tilde{N}) + i\eta k_{\perp}^2\tilde{\chi} = 0, \tag{10}$$

where $\tilde{N} = N/N$, $\tilde{U}_{\parallel} = U_{\parallel i}/C_s$, $\tilde{\varphi} = e\varphi/T_e$, and $\tilde{\chi} = eA_{\parallel}C_s/T_e$ are four normalized perturbed quantities representing plasma density, parallel flow of combined fluid (in center of mass reference frame), electrostatic potential and parallel component of vector potential, respectively. Where, $\boldsymbol{\Omega_{\kappa}}$ is the contribution of the frequency to the drift wave that is associated with the curvature effect due to effective gravitational force. Here, $C_A^2 = B^2/4Nm_i$ is propagation velocity of Alfven wave, μ represents viscosity and $\rho_i^2 = T_i m_i/e^2B^2$ is the Larmor radius of ion.

Defining new variables $W = \tilde{\varphi} - \tilde{N}$ and $X = (\Omega/\Omega_{*e})\tilde{N} - \tilde{\varphi}$ and eliminating the vector potential $\tilde{\chi}$ and parallel velocity flow $\tilde{U}_{\parallel}$ from Eqs. (7), (8), (9), and (10) coupled equations of shear Alfven wav,.

$$\frac{iC_s k_{\parallel}}{\Omega_s}\left[\frac{(\Omega - \Omega_{*e})k_{\perp}}{\Omega - \Omega_{*e} + i\Omega_{\eta}k_{\perp}^2}\left(\frac{iC_s k_{\parallel}}{\Omega_s}\right)W\right] - \frac{\left(\Omega - \frac{\Omega_{\kappa}\Omega_A^2}{\Omega_s^2}\right)(\Omega - i\Omega_{\mu}k_{\perp}^2)}{\Omega_A^2}k_{\perp}^2$$
$$W - \frac{\frac{2\Omega_{\kappa}\Omega_A^2}{\Omega_s^2(\Omega + i\Omega_{\mu}k_{\perp}^2)}}{\Omega_A^2}k_{\perp}^2 X = 0, \tag{11}$$

and drift acoustic wave,

$$-\frac{C_s^2 k_{\parallel}^2}{\Omega_s^2}X + \frac{(\Omega - \Omega_{*e})(\Omega + 4i\Omega_{\mu}k_{\perp}^2)}{\Omega_s^2}X - \left[4q^2(\Omega + 4i\Omega_{\mu}k_{\perp}^2)\right.$$
$$\left.\left(\frac{1}{\Omega_A^2} + \frac{2\Omega\Omega_{*e}}{\Omega_A^4}k_{\perp}^2\right) + \frac{i\Omega_{\eta}k_{\perp}^2(\Omega + i\Omega_{\eta}k_{\perp}^2)}{\Omega_A^2(\Omega - \Omega_{*e})}\right]\left[(\Omega - \Omega_{\kappa}\Omega_A^2/\Omega_s^2)W - \right.$$
$$\left.(2\Omega_{\kappa}\Omega_A^2/\Omega_s^2)X\right] - \left[\frac{i\Omega_{\eta}}{(\Omega - \Omega_{*e})} - \frac{i\Omega_{\eta}k_{\perp}^2(\Omega + 4i\Omega_{\mu}k_{\perp}^2)}{\Omega_A^2}\right](W + X) -$$
$$\frac{iC_s k_{\parallel}}{\Omega_s}\left[\frac{1}{(\Omega + 4i\Omega_{\mu}k_{\perp}^2)}\right]\left[\frac{i\Omega_{\eta}k_{\perp}^2}{\Omega - \Omega_{*e} + i\Omega_{\eta}k_{\perp}^2}\frac{iC_s k_{\parallel}}{\Omega_s}W + \frac{iC_s k_{\parallel}}{\Omega_s}X\right] = 0 \tag{12}$$

are obtained. Excluding the viscosity ($\mu \to 0$) and discarding the diamagnetic drift ($\Omega_{*e}/\Omega \to 0$), these equations reduce to single fluid resistive MHD model.

3. Calculations

In the tokamak plasmas edge region, the resistive diffusion time scale ($\tau_{\eta} = 4\pi L^2/\eta c^2$) is longer than Alfven time scale ($\tau_A = 1/\Omega_A$) and the growth-rate scale as fractional power of resistivity ($\gamma \sim \eta^{1/3}$). Therefore, the inverse Lundquist number (τ_A/τ_{η}) satisfies the condition $\varepsilon_{\eta}^3 = \tau_A/\tau_{\eta} \ll 1$. Furthermore, we assume that the mode frequency and growth-rate of the resistive coupled modes are satisfying the ordering $\Omega \sim \gamma \sim \Omega_s \sim \Omega_{*e} \sim \Omega_{\kappa} \sim \varepsilon_{\eta}\Omega_A$. Viscosity is less than or equal to resistivity $\Omega_{\mu} \le \Omega_{\eta} = \varepsilon_{\eta}^3\Omega_A$. Introducing a slow variable $Y = \varepsilon_{\eta}k_{\parallel}$, we may write $\frac{iC_s k_{\parallel}}{\Omega_s} \to \frac{iC_s k_{\parallel}}{\Omega_s} + \varepsilon_{\eta}\partial/\partial Y$ and expand equations as;

$$W(k_{\parallel}, Y) = W_0(k_{\parallel}, Y) + \varepsilon_{\eta}W_1(k_{\parallel}, Y) + \ldots\ldots\ldots\ldots, \tag{13}$$

$$X(k_{\parallel}, Y) = \varepsilon_{\eta}X_1(k_{\parallel}, Y) + \varepsilon_{\eta}^2 X_2(k_{\parallel}, Y) + \ldots\ldots\ldots\ldots, \tag{14}$$

The equation for leading order eigen-function is given as;

$$\frac{\frac{d}{dY}\left[(\overline{\Omega} - \overline{\Omega}_{*e})Y^2\right.}{\left.(\overline{\Omega} - \overline{\Omega}_{*e}) + iY^2\frac{dW_0}{dY}\right] + (\overline{\Omega} - \overline{\Omega}_{\kappa})(\overline{\Omega} + i\overline{\mu}Y^2)Y^2W_0 = 0,} \tag{15}$$

where $\overline{\Omega} = \Omega/\varepsilon_{\eta}\Omega_A$, $\overline{\Omega}_{*e} = \Omega_{*e}/\varepsilon_{\eta}\Omega_A$, $\overline{\Omega}_{\kappa} = \Omega_{\kappa}/\varepsilon_{\eta}\Omega_A$, $\overline{\Omega}_s = \Omega_s/\varepsilon_{\eta}\Omega_A$ and $\overline{\mu} = \Omega_{\mu}/\Omega_{\eta}$. The Eq. (15) subject to boundary conditions $W_0(Y \to \infty) = 0$ and $W_0(Y \to 0) = L_B^{-1} + \varepsilon_{\eta}Y^{-1}$. To obtain dispersion relation for coupled resistive modes, we introduce another secular variable $Z^2 = iY^2/(\overline{\Omega} - \overline{\Omega}_{*e})$ which yields,

$$\frac{d}{dZ}\left[\frac{Z^2}{1 + Z^2}\frac{dW_0}{dZ}\right] - \left[Z^2A(Z^2) + Z^4B(Z^2)\right]W_0 = 0 \tag{16}$$

where $A(Z^2) = i\overline{\Omega}(\overline{\Omega} - \overline{\Omega}_{\kappa})(\overline{\Omega} - \overline{\Omega}_{*e})(1 + 2q^2C(Z^2))$, $B(Z^2) = i\overline{\mu}(\overline{\Omega} - \overline{\Omega}_{\kappa})(\overline{\Omega} - \overline{\Omega}_{*e})(1 + 8q^2C(Z^2))$, and $C(Z^2) = \overline{\Omega}_s/\overline{\Omega}_s^2(\overline{\Omega} - \overline{\Omega}_{*e})[\overline{\Omega} + 4\overline{\mu}(\overline{\Omega} - \overline{\Omega}_{*e})Z^2]$.

4. Results and discussion

For the non-viscous plasma, Eq. (16) take the following form;

$$\frac{d}{dZ}\left[\frac{Z^2}{1 + Z^2}\frac{dW_0}{dZ}\right] - A_0Z^2W_0 = 0 \tag{17}$$

where $A_0 = i\overline{\Omega}(\overline{\Omega} - \overline{\Omega}_{\kappa})(\overline{\Omega} - \overline{\Omega}_{*e})(1 + 2q^2C_0)$, in which $C_0 = \overline{\Omega}_s^2/\{\overline{\Omega}_s^2 - \overline{\Omega}(\overline{\Omega} - \overline{\Omega}_{*e})\}$, and equation is subject to boundary condition $W_0(Z \to \infty) = 0$ and $W_0(Z \to 0) = L_B^{-1} + (i/(\overline{\Omega} - \overline{\Omega}_{*e}))^{1/2}\varepsilon_{\eta}Z^{-1}$. Using above mentioned conditions, we finally get the dispersion relation for coupled macro and micro mode with localized influence of two-fluid effect:

$$-i(\overline{\Omega} - \overline{\Omega}_{\kappa})\left[(1 + 2q^2)\overline{\Omega}_s^2 - \overline{\Omega}(\overline{\Omega} - \overline{\Omega}_{*e})\right] - \frac{L_n^{'2}}{2}\Omega_{\eta}\Omega_A = 0, \tag{18}$$

where $L_n^{'} = (2\mu_0Lq^2/B^2)dp/dx$, $\overline{\Omega}_{\kappa}$ is the ion magnetic drift frequency, Ω_A is the Alfven wave frequency (ensures the global MHD mode), $\overline{\Omega}_{*e}$ is the electron diamagnetic drift frequency (preserves the local drift wave dynamics), Ω_{η} is the inverse of resistive time scales (retain resistive drives for both local and global mode). The three roots of Eq. (18) reflects the waves propagation of the ion drift wave, the coupled drift-acoustic wave and the Alfven wave, as shown in Figure 1. The solid red curve in Figure 1, is the real part of unstable root, which escort the frequency of Alfven wave at the lower values of perpendicular wave number $k_{\perp}$, and asymptotically it goes toward the electrostatic electron drift-acoustic mode for higher values of $k_{\perp}$. The dotted black and the dashed blue curves are the other two roots of Eq. (18), representing the drift frequency due to ion and electron respectively. The coupling of electron drift-acoustic mode can be discarded at $\Omega_s \to 0$ (Scott 1997). Well-known drift ballooning mode (Rafiq et al. 2009) can be retrieved in the self-sustained curvature effect, for example in toroidal symmetry (subsided effective ion curvature drift at $\overline{\Omega}_{\kappa} \to 0$). It is interesting to observe from Figure 1 that the coupling of the real part of unstable mode occurs with the ion drift and electron drift frequencies.

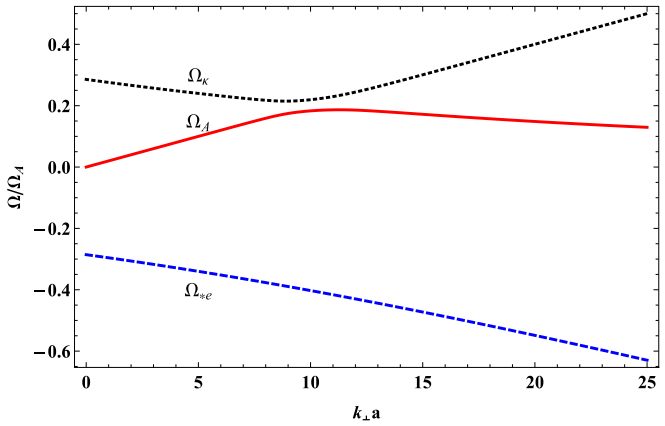

Figure 1. Frequencies of the all three modes of plasma obtained from the roots of Eq. (18). The solid red curve represents the real part of resistive drift ballooning mode against perpendicular mode number, $k_\perp a$ at plasma parameters, $q = 5$ and $\Omega_k/k_\perp U_A = 0.02$.

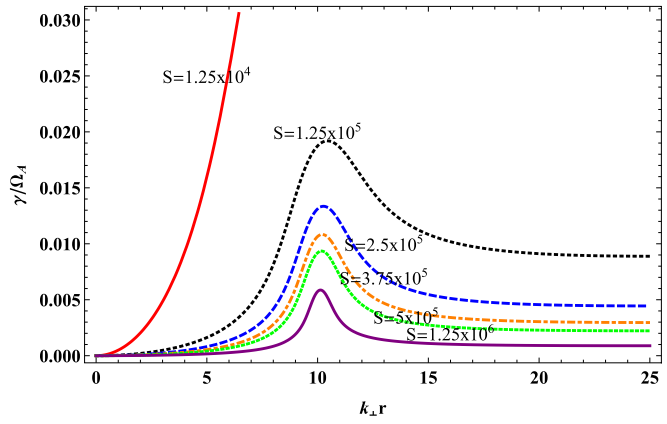

Figure 2. Growth rate of the resistive drift ballooning mode [imaginary part of unstable root from Eq. (18)] against perpendicular mode number, $k_\perp a$. Plasma parameters are, $q = 5$, $\Omega_k/k_\perp U_A = 0.02$, and $L_n^{'} = 1$.

Table 1 provides essential plasma parameters where the coupling in the modes could play a significant role at tokamak edge regime (Scott 1997). The growth rate of the coupled modes (imaginary part of the unstable root) is depicted in Figure 2. The ballooning mode can be characterized as the destabilized Alfven mode by curvature forcing. As the normalized perpendicular wave-number from $k_\perp r = 0$ to $k_\perp r = 10$ have increased, the growth rate is rising from zero to maximum. Figure 2 explores the variation of the growth-rate against perpendicular wave-number $k_\perp r$for different values of resistivity (in terms of the Lundquist number S). The mode grows exponentially at$S = 1.25 \times 10^4$, while at moderate values$1.25 \times 10^5 \leq S \leq 5 \times 10^5$, the mode is localized between $5 \leq k_\perp r \leq 15$. Further increase of the Lundquist number at $S \geq 1.25 \times 10^5$, contributes to mode stabilization as shown in Figure 2.

The dispersion relation given in Eq. (18) is the generalized dispersion relation, which admits variety of modes such as drift mode, coupled drift-Alfven mode, Alfven mode, MHD ideal ballooning mode, two-fluid ballooning mode and associated resistive modes. The parallel and perpendicular dynamics, and physical plasma parameters determine which linear mode will dominate. Contour plots of the growth rate (γ,$k_\perp r$, S) are shown in Figure 3. The unstable modes are found at low values of$k_\perp r$, while the scan unstable modes are numerically solved for the Lundquist number in the range$10^4 \leq S \leq 10^5$.

To demonstrate the two fluid effect through ion drift or electron acoustic-drift on ideal modes, we have considered the ideal ballooning instability i.e.$L_B^{-1} < 0$, $\mu \to 0$ and$\eta \to 0$.The Eq. (17), gives

$$-\overline{\Omega}(\overline{\Omega}-\overline{\Omega}_\kappa)\left[(1+2q^2)\overline{\Omega}_s^2-\overline{\Omega}(\overline{\Omega}-\overline{\Omega}_{*e})\right]-\left(\frac{\Omega_A}{L_B}\right)^2\left\{\overline{\Omega}_s^2-\overline{\Omega}(\overline{\Omega}-\overline{\Omega}_{*e})\right\}=0 \tag{19}$$

Table 1. Plasma parameters used in analytical and numerical calculations.

Parameter	Symbol	Typical Value Used
Density	N	$10^{17} m^{-3}$
Magnetic field	B	0.1 T
Temperature	T	6.5 eV
Ion gyration frequency	ω_{ci}	$\sim 10^7$ rad/s
Ion acoustic speed	C_s	$\sim 10^4$ m/s
Alfven speed	C_A	$\sim 10^6$ m/s
Characteristic length scale	a	0.1m
Ion Larmor radius	ρ_i	2.5mm
Resistivity	η	$\sim 10^{-5}$Ohm-m

here, L_B^{-1} contains ideal ballooning instability source along with three oscillation modes; the ions drift mode$\overline{\Omega} = \overline{\Omega}_\kappa$ the electron drift-acoustic mode $\overline{\Omega}(\overline{\Omega} - \overline{\Omega}_{*e}) = (1 + 2q^2)\overline{\Omega}_s^2$. It is noted that the optimal ballooning mode is stabilized by increasing the two-fluid effect (through increasing the diamagnetic drift frequencies) as shown in Figure 4 (a). Growth rate contour plots$\gamma(k_\perp r, L_B^{-1})$, obtained from the dispersion relation Eq. (19) are shown in Figure 4 (b). The most unstable mode continuum are located in the moderate range of perpendicular wave numbers. In the edge plasma, the ideal ballooning mode (Hastie et al. 2003) can be recovered as a special case at $\overline{\Omega}_\kappa \to 0$.

Two-fluid effects adequately modify the spectrum of the mode when the drift-acoustic wave coupling includes the finite values of the frequency of sound wave propagation. The growth-rate is plotted against perpendicular wave number $k_\perp a$ at frequency of sound wave ($\overline{\Omega}_s = 0.05\Omega_A$). It is observed that modes are stabilized at low and high perpendicular wave numbers. By solving Eq. (19) numerically, a localized continuum of unstable modes (island of instability) are explored for the moderate range of perpendicular wave number (see Figure 5). The Linear characteristics of the coupled mode (Eq. (18)) are significantly altered by neglecting the curvature effect i.e.$L_B^{-1} \to 0$. In this case, the localized coupled resistive-drift-acoustic-mode has been verified, which is the analogue to the well-known drift wave instability (Yang et al., 2018)

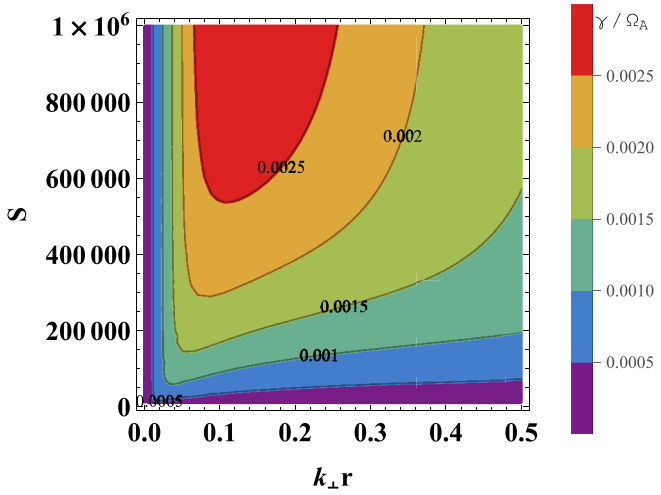

Figure 3. The contour plots of the growth rate dependence $\gamma(k_\perp a, S)$ generated from generalized dispersion relation, from Eq. (18), parameters are $q = 5$, $\Omega_k/k_\perp U_A = 0.02$, and $L_n^{'} = 1$.

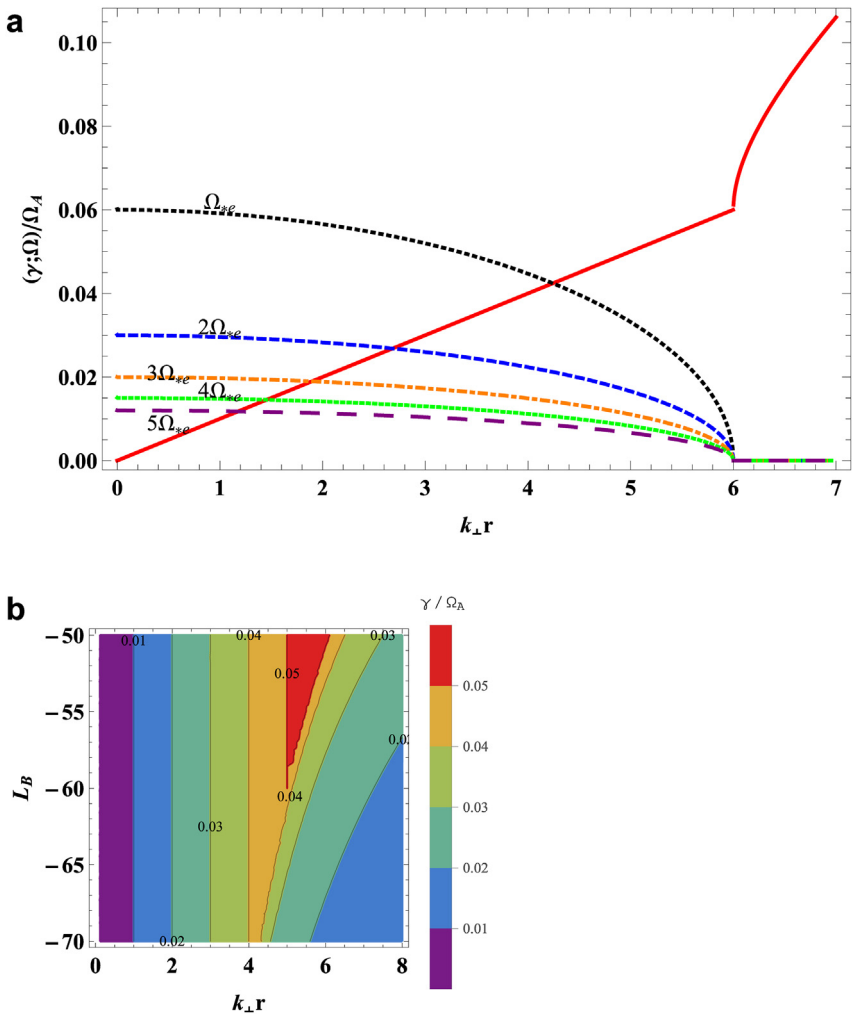

Figure 4. (a) Variation of real (the solid red curve) and imaginary (dot-dashed curves) parts of unstable mode, from Eq. (19), where the plasma parameters are q = 1, $\Omega_k/k_\perp U_A = 0.02$ and$L_B^{-1} = -50$. (b) The contour plots of the growth rate dependence $\gamma(k_\perp a, L_B^{-1})$ from Eq. (18), other parameters are same as in Figure 4 (a).

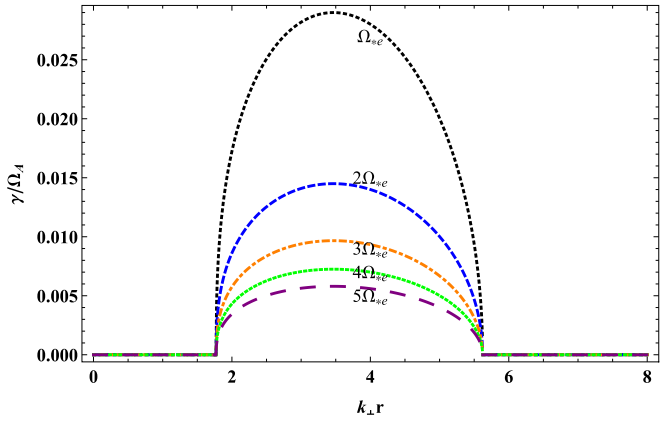

Figure 5. Two-fluid-modified ideal ballooning normalized-growth-rate, against $k_\perp a$ for $\Omega_s/\Omega_A = 0.05$, other parameters are same as in Figure 4.

$$\left[i\overline{\Omega}^2(\overline{\Omega}-\overline{\Omega}_{*e})-i\left(1+2q^2\right)\overline{\Omega\Omega}_s^2-\right]-\frac{L_n'^2}{2}\Omega_\eta\Omega_A=0. \tag{20}$$

To demonstrate the linear dispersion properties of resistive drift waves, Eq. (20) is numerically solved by considering parameters related to edge fusion plasma environment (Nascimento F., & Machida, M. 2012) as given in Table 1. The mechanism of resistive drift instability is the phase shift in the fluctuation of density and potential due to electron collisions with ions. The roots of Eq. (20) reflects the propagation of three waves, the ion drift, the electron drift, and the acoustic wave propagation, as shown in Figure 6. The dotted-dashed curves represent growth-rate of the unstable modes at different values of resistivity parameter S. There are two pathways in pressure driven instabilities for free energy to excite the mode, one is drift mode mechanism which makes cross-coupling among pressure, parallel current and potentials through parallel dynamics in $k_\parallel$-space, and the other is MHD mechanism which couples pressure with potential via. Curvature forcingL_B^{-1}. One of our objectives is to find out which mode is dominant in the $k_\perp$-space continuum. Only drift mode dynamics are present if we exclude curved magnetic fluctuations at $\Omega_\kappa = 0$ by taking$L_B^{-1} \to 0$. These two modes are different in coupling mechanism, the spectra of the gradient drive, dissipative resistance, cross-coherence and shifting of phase is reflected in modes.

The three dimensional plots of the growth rate $\gamma(k_\perp r, S)$ obtained from Eq. (20) are shown in Figure 7. The most unstable modes are found in the lower values of Lundquist number S and higher range of perpendicular wave number.

It is observed that for given collisionality, all states of L-H transition lie under the resistive drift-Alfven regimes and are stable to ideal ballooning mode (see ref: Scott, 1997). The two-fluid MHD model is

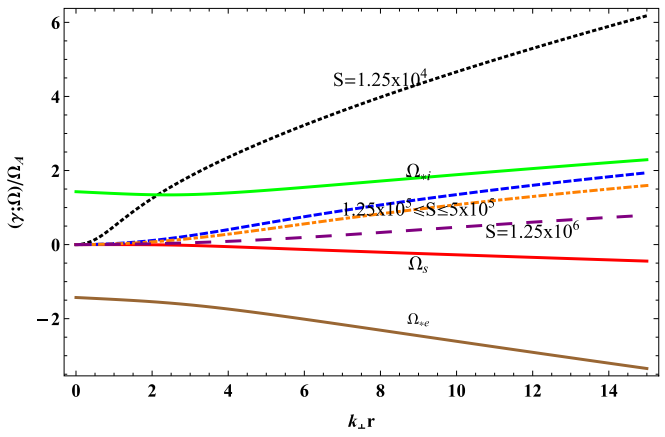

Figure 6. Frequencies of the all three modes of plasma obtained from the roots of Eq. (20). The solid curves (green→ ion-diamagnetic-drift wave, red→ ion-acoustic wave, brown→ electron-diamagnetic-drift wave) represent the real parts of the DWI against perpendicular mode number, $k_\perp a$. Whereas, the dotted and dashed curves represent the imaginary part of unstable root at $\Omega_s/\ \Omega_A = 0.001$ and $L_n^{'} = 1.10$ for different values of Lundquist number S.

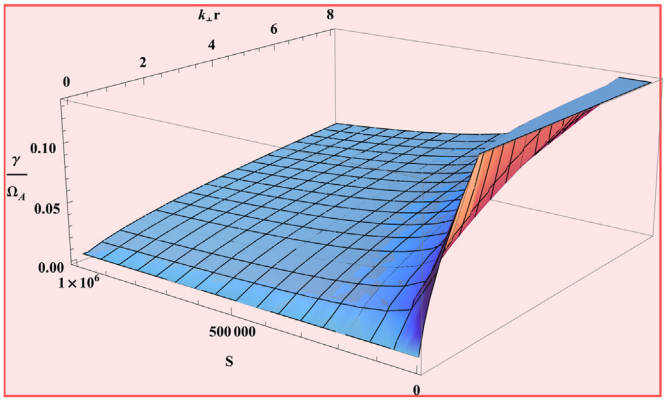

Figure 7. The plots of the growth rate dependence $\gamma(k_\perp a, S)$ generated from generalized dispersion relation, from Eq. (20) at $\Omega_s/\Omega_A = 0.001$ and $L_n^{'} = 1.10$.

extensively used by plasma community (Wagner et al. 1982; Gohil et al. 1994; Connor and Wilson 2000; ASDEX team 1989; Righi et al. 1999; Chankin 1997; Marashek et al. 1997; Shikui Cheng et al., 2019) to describe fundamental theory of fusion plasma and rapid revival of interest with computational calculations is observed (Shen et al. 2020; Ren et al. 2020; Zhu and Reader 2013; Cheng et al. 2017; Xi et al. 2012; Meneghini et al. 2015). The four field plasma model has been introduced to describe the coupling effects of microscopic and macroscopic dynamics for edge regime tokamak plasma. The four field plasma model has significance and advantage in terms of self-consisting coupling mechanism of micro and macroscopic dynamics of plasmas over two-fluid MHD model. In the two-fluid MHD, approximation of inertia-less electron leads to a question on energy conservation.

5. Summary

The new dispersion relation has been derived to estimate growth rate of the coupled unstable modes, originated due to the coexistence of macro and micro level dynamics in the tokamak edge plasma region (with same source of free energy, i.e. pressure gradient). The four-field plasma model, which includes both macroscopic and microscopic dynamics for the coupled modes, has been presented in this paper. The key effects related to tokamak edge plasma environment such as two-fluid effects (ion curvature drift, electron diamagnetic drift), dissipation effect (resistivity due to collision) and coupling effect due to interaction with acoustic mode are incorporated. The ion drift wave, the electron diamagnetic drift wave and the Alfven wave are the real roots of the coupled equation. The imaginary part of unstable modes have been explored and the growth-rate are estimated at different values of resistivity. Ion drift is found to affect the dynamics of the unstable modes due to curvature in the magnetic field.

Declarations

Author contribution statement

Umer Rehman: Conceived and designed the experiments; Performed the experiments; Analyzed and interpreted the data; Contributed reagents, materials, analysis tools or data; Wrote the paper.

Ahmad Ali: Analyzed and interpreted the data; Contributed reagents, materials, analysis tools or data.

Shakeel Mahmood: Contributed reagents, materials, analysis tools or data.

Funding statement

This research did not receive any specific grant from funding agencies in the public, commercial, or not-for-profit sectors.

Data availability statement

Data included in article/supplementary material/referenced in article.

Declaration of interests statement

The authors declare no conflict of interest.

Additional information

No additional information is available for this paper.

Acknowledgements

The first author would like to thank Prof. F. Porcelli, Prof. Wang Shaojie, and Prof. P. Zhu for constructive suggestions on the subject and learning fusion plasma physics during stay at USTC, Hefei China. We are also thankful to Dr. Rubina Nasir for carefully reading and improving the quality of English language.

References

ASDEX team, 1989. The H-mode of ASDEX. Nucl. Fusion 29, 1959.
Beer, M.A., Cowley, S.C., Hammett, G.W., 1995. Field-aligned coordinates for nonlinear simulations of tokamak turbulence. Phys. Plasmas 2, 2687.
Bessenrodt-Weberpals, M., et al., The ASDEX Team, ICRH Team, LH Team, NI Team, Pellet Injection Team, PSI Group, 1993. The isotope effect in ASDEX. Nucl. Fusion 33, 1205.
Bisai, N., Santanu, Banerjee, Abhijit, Sen, 2019. A universal mechanism for plasma blob formation. Phys. Plasmas 26, 020701.
Biskamp, B., Walter, M., 1985. Suppression of shear damping in drift wave turbulence. Phys. Lett. A 109, 34–38.
Callen, J.D., 1977. Drift-wave turbulence effects on magnetic structure and plasma transport in tokamaks. Phys. Rev. Lett. 39, 1540.
Camargo, S.J., Biskamp, D., Scott, B.D., 1995. Resistive drift-wave turbulence. Phys. Plasmas 2, 48.
Carreras, B.A., Diamond, P.H., 1989. Thermal diffusivity induced by resistive pressure-gradient-driven turbulence. Phys. Fluids B 1, 1011.
Carreras, B.A., et al., 1983. Transport effects induced by resistive ballooning modes and comparison with high-βp ISX-B tokamak confinement. Phys. Rev. Lett. 50, 503.
Carreras, B.A., Garcia, L., Diamond, P.H., 1987. Theory of resistive pressure-gradient-driven turbulence. Phys. Fluids 30, 1388.
Chankin, A.V., 1997. Critical parameters for turbulent transport in the SOL: mechanism for the L - H transition and its impact on the H-mode power threshold and density limits. Plasma Phys. Contr. Fusion 39, 1059.

Cheng, S., Zhu, P., Banerjee, D., 2017. Enhanced toroidal flow stabilization of edge localized modes with increased plasma density. Phys. Plasmas 24, 092510.
Cheng, S., et al., 2019. Dominant two-fluid magnetohydrodynamic instabilities in CFETR upgrade phase-I scenario in presence of perfect conducting wall. Plasma Phys. Contr. Fusion 61, 045009.
Connor, J.W., Wilson, H.R., 2000. A review of theories of the L-H transition. Plasma Phys. Contr. Fusion 42, 1.
Connor, J.W., Hastie, R.J., Taylor, J.B., 1978. Shear, periodicity, and plasma ballooning modes. Phys. Rev. Lett. 40, 396.
Connor, J.W., Hastie, R.J., Wilson, H.R., 1998. Magnetohydrodynamic stability of tokamak edge plasmas. Phys. Plasmas 5, 2687.
Coppi, B., 1977. Topology of ballooning modes. Phys. Rev. Lett. 39, 939.
Cowley, S.C., Kulsrud, R.M., Sudan, R.N., 1991. Considerations of ion-temperature-gradient-driven turbulence. Phys. Fluids B 3, 2767.
Dewar, R.L., Glasser, A.H., 1983. Ballooning mode spectrum in general toroidal systems. Phys. Fluids 26, 3038.
Dobrott, D., et al., 1977. Theory of ballooning modes in tokamaks with finite shear. Phys. Rev. Lett. 39, 943.
Easy, L., Militello, F., Omotani, J., Dudson, B., Havlíčková, E., Tamain, P., Naulin, V., Nielsen, A.H., 2014. Three dimensional simulations of plasma filaments in the scrape off layer: a comparison with models of reduced dimensionality. Phys. Plasmas 21, 122515.
Fridberg, J.P., 2014. Ideal Magnetohydrodynamics. Cambridge University Press.
Furno, I., Labit, B., Podestà, M., Fasoli, A., Müller, S.H., Poli, F.M., Ricci, P., Theiler, C., Brunner, S., Diallo, A., Graves, J., 2008. Experimental observation of the blob-generation mechanism from interchange waves in a plasma. Phys. Rev. Lett. 100, 055004.
Galeev, A.A., Moiseev, S.S., Sagdeev, R.Z., 1964. Theory of stability of nonhomogeneous plasmas and anomalous diffusion. J. Nucl. Energy Part C 6645.
Gohil, P., Burrell, K.H., Doyle, E.J., Groebner, R.J., Kim, J., Seraydarian, R.P., 1994. The phenomenology of the L-H transition in the DIII-D tokamak. Nucl. Fusion 34, 1057.
Graessle, D.E., Prager, S.C., Dexter, R.N., 1989. Tokamak magnetic turbulence over the safety-factor range $0.6<q<3$. Phys. Rev. Lett. 62, 535.
Guzdar, P.N., et al., 2001. Zonal flow and zonal magnetic field generation by finite β drift waves: a theory for low to high transitions in tokamaks. Phys. Rev. Lett. 87, 015001.
Hasegawa, A., Mima, K., 1977. Stationary spectrum of strong turbulence in magnetized nonuniform plasma. Phys. Rev. Lett. 39, 205.
Hasegawa, A., Mima, K., 1978. Pseudo-three-dimensional turbulence in magnetized nonuniform plasma. Phys. Fluids 21, 87.
Hasegawa, A., Wakatani, M., 1982. Plasma edge turbulence. Phys. Rev. Lett. 50, 682.
Hastie, R.J., Ramos, J.J., Porcelli, F., 2003. Drift ballooning instabilities in tokamak edge plasmas. Phys. Plasmas 10, 4405.
Hegna, C.C., Hudson, S.R., 2002. Ideal magnetohydrodynamic ballooning stability boundaries in three-dimensional equilibria. Phys. Plasmas 9, 2014.
Hender, T.C., et al., 1984. The effects of compressibility of the resistive ballooning mode. Phys. Fluid. 27, 1439.
Hirose, A., Zhang, L., Elia, M., 1994. Higher order collisionless ballooning mode in tokamaks. Phys. Rev. Lett. 72, 3993.
Horton, W., 1990. Nonlinear drift waves and transport in magnetized plasma. Phys. Rep. 192, 1–177.
Hubbard, A.E., Boivin, R.L., Granetz, R.S., et al., 2001. Pedestal profiles and fluctuations in C-Mod enhanced D-alpha H-modes. Phys. Plasmas 8, 2033.
Kikuchi, M., Azumi, M., 2015. Frontiers in Fusion Research II. Springer International Publishing.
Lee, W., Angus, J.R., Umansky, M.V., Krasheninnikov, S.I., 2015a. Electromagnetic effects on plasma blob-filament transport. J. Nucl. Mater. 463, 765–768.
Lee, W., Umansky, M.V., Angus, J.R., Krasheninnikov, S.I., 2015b. Electromagnetic effects on dynamics of high-beta filamentary structures. Phys. Plasmas 22, 012505.
Lee, W., Angus, J.R., Krasheninnikov, S.I., 2015c. Electromagnetic drift waves dispersion for arbitrarily collisional plasmas. Phys. Plasmas 22, 072113.
Liewer, P.C., 1985. Measurements of microturbulence in tokamaks and comparisons with theories of turbulence and anomalous transport. Nucl. Fusion 27, 611.
Marashek, M., Gunter, S., Kass, T., Scott, B., Zohm, H., ASDEX upgrate team, 1997. Observation of toroidicity-induced alfvén eigenmodes in ohmically heated plasmas by drift wave excitation. Phys. Rev. Lett. 79, 4186.
McCarthy, D.R., et al., 1992. Stability of resistive and ideal ballooning modes in the Texas Experimental Tokamak and DIII-D. Phys. Fluids B 4, 1846.
Meneghini, O., et al., 2015. Integrated modeling applications for tokamak eperiments with OMFIT. Nucl. Fusion 55, 083008.
Mikhailovskii, A.B., Rudakov, L.I., 1963. The stability of a spatially inhomogeneous plasma in a magnetic field. Sov. Phys. - JETP 17, 621. http://www.jetp.ac.ru/cgi-bin/dn/e_017_03_0621.pdf.
Myra, J.R., D'Ippolito, D.A., Xu, X.Q., Cohen, R.H., 2000. Resistive modes in the edge and scrape-off layer of diverted tokamaks. Phys. Plasmas 7, 4622.
Nascimento, F do, Machida, M., 2012. Measurements of plasma edge electron temperature and density using visible spectroscopy in NOVA-UNICAMP tokamak. J. Phys. Conf. 370, 012053.
Park, J.K., et al., 2018. 3D field phase-space control in tokamak plasmas. Nat. Phys. 14, 1223–1228.
Rafiq, T., Hegna, C.C., Callen, J.D., Kritz, A.H., 2009. Unified theory of resistive and inertial ballooning modes in three-dimensional configurations. Phys. Plasmas 16, 102505.
Rehman, U., 2019. Electromagnetic viscous-resistive-drift-wave instability in burning plasma. J. Fusion Energy 38, 531.
Ren, H., et al., 2020. Excitation of zonal flow by nonlinear geodesic acoustic mode. Phys. Plasmas 27, 034501.
Righi, E., et al., 1999. Isotope scaling of the H mode power threshold on JET. Nucl. Fusion 39, 309.
Rogers, B.N., Drake, J.F., 1997. Enhancement of turbulence in tokamaks by magnetic fluctuations. Phys. Rev. Lett. 79, 229.
Rogers, B.N., Drake, J.F., 1999. Diamagnetic stabilization of ideal ballooning modes in the edge pedestal. Phys. Plasmas 6, 2797.
Scott, B.D., 1990. Self-sustained collisional drift-wave turbulence in a sheared magnetic field. Phys. Rev. Lett. 65, 3289.
Scott, B., 1997. Three-dimensional computation of drift Alfvén turbulence. Plasma Phys. Contr. Fusion 39, 1635.
Scott, B.D., Biglari, H., Terry, P.W., Diamond, P.H., 1991. Self-organization in sheared drift-wave turbulence. Phys. Fluids B 3, 51.
Shen, N., et al., 2020. Magnetohydrodynamic Richtmyer–Meshkov instability under an arbitrarily oriented magnetic field. Phys. Plasmas 27, 062101.
Strauss, H.R., 1976. Nonlinear three-dimensional magnetohydrodynamics of noncircular tokamaks. Phys. Fluids 19, 134.
Strauss, H.R., 1981. Resistive ballooning modes. Phys. Fluids 24, 2004.
Sykes, A., Bishop, C.M., Hastie, R.J., 1987. Resistive ballooning modes and the second region of stability. Plasma Phys. Contr. Fusion 29, 719.
Todd, A.M.M., et al., 1976. Stability limitations on high-beta tokamaks. Phys. Rev. Lett. 38, 826.
Wagner, F., et al., 1982. Regime of improved confinement and high beta in neutral-beam-heated divertor discharges of the ASDEX tokamak. Phys. Rev. Lett. 49, 1408.
Wakatani, M., Hasegawa, A., 1984. A collisional drift wave description of plasma edge turbulence. Phys. Fluids 27, 611.
Waltlz, R.E., 1985. Numerical simulation of electromagnetic turbulence in tokamaks. Phys. Fluid. 28, 577.
Weiland, J., 2000. Collective Modes in Inhomogeneous Plasma IOP. Bristol, Philadelphia and New York.
Wootton, A.J., Carreras, B.A., Matsumoto, H., McGuire, K., Peebles, W.A., Ritz, Ch.P., Terry, P.W., Zweben, S.J., 1990. Fluctuations and anomalous transport in tokamaks. Phys. Fluids B 2, 2879.
Xi, P.W., Xu, X.Q., Wang, X.G., Xia, T.Y., 2012. Influence of equilibrium shear flow on peeling-ballooning instability and edge localized mode crash. Phys. Plasmas 19, 092503.
Xu, X.Q., Cohen, R.H., et al., 2000. Turbulence studies in tokamak boundary plasmas with realistic divertor geometry. Nucl. Fusion 40, 3Y.
Xu, X.Q., Cohen, R.H., Rognlien, T.D., Myra, J.R., 2000. Low-to-high confinement transition simulations in divertor geometry. Phys. Plasmas 7, 1951.
Xu, J.Q., Peng, X.D., Hao, G.Z., Qu, H.P., Chen, W., Li, J.Q., 2021. Impurity effect on drift-resistive-inertial ballooning mode and associated transport at the edge of tokamak plasmas. Phys. Plasmas 28, 012505.
Yang, S.C., Zhu, P., Xie, J., Liu, W., 2018. Two-fluid MHD regime of resistive drift-wave instability. Phys. Plasmas 25, 092113.
Zeiler, A., Biskamp, D., Krake, J.F., Guzdar, P.N., 1996. Three-dimensional fluid simulations of tokamak edge turbulence. Phys. Plasmas 3, 2951.
Zeiler, A., Drake, J.F., Rogers, B., 1997. Nonlinear reduced Braginskii equations with ion thermal dynamics in toroidal plasma. Phys. Plasmas 4, 2134.
Zhu, P., Reader, J., 2013. Plasmoid formation in current sheet with finite normal magnetic component. Phys. Rev. Lett. 110, 235005.